# Metabolic FLIM of Macroscopic Objects

*Wolfgang Becker, Lukas Braun, Julius Heitz, Becker & Hickl GmbH, Berlin*
*Vladislav Shcheslavskiy, Marina Shirmanova, Privolzhski Research Medical University, Nizhniy Novgorod*

*Abstract:* Fluorescence lifetime images of macroscopic samples as large as 20 mm can be recorded in the primary focal plane of the DCS-120 confocal scanner. The system can be used for measuring metabolic parameters of biological tissue. Metabolic FLIM is performed via the fluorescence decay parameters of NAD(P)H and thus requires an excitation wavelength of 375 nm or shorter. Commonly used lens elements have poor transmission and large chromatic aberration at this wavelength. We therefore replaced the standard scan lens with one that consists of a combination of UV achromats. This increases the efficiency of the system by 40%. The spatial resolution is about 15 µm, images can be recorded with pixel numbers as large as 2048 x 2048. Acquisition times range from a few seconds for imaging with low pixel number and moderate lifetime accuracy to a few minutes for mega-pixel images and ultra-high accuracy of the decay data. We demonstrate the use of the system for metabolic imaging of a tumor in a mouse and of glioblastoma in a rat brain.

## Motivation

FLIM, especially TCSPC FLIM, is usually associated with imaging through a laser scanning microscope [2, 3]. A laser beam is sent down the beam path of the microscope, and scanned around a pivot point located in the principle plane of the microscope lens. The fluorescence light is collected back through the microscope lens and the scanner, separated from the excitation light by a dichroic mirror, and detected through a pinhole [3, 4]. Microscopes are usually limited to an image size of no more than 500 x 500 µm. To perform FLIM of larger objects bh have introduced the DCS-120 MACRO system [3, 4]. Instead of imaging through a microscope, this system scans the object directly in the image plane of the scanner. An example is shown in Fig. 1.

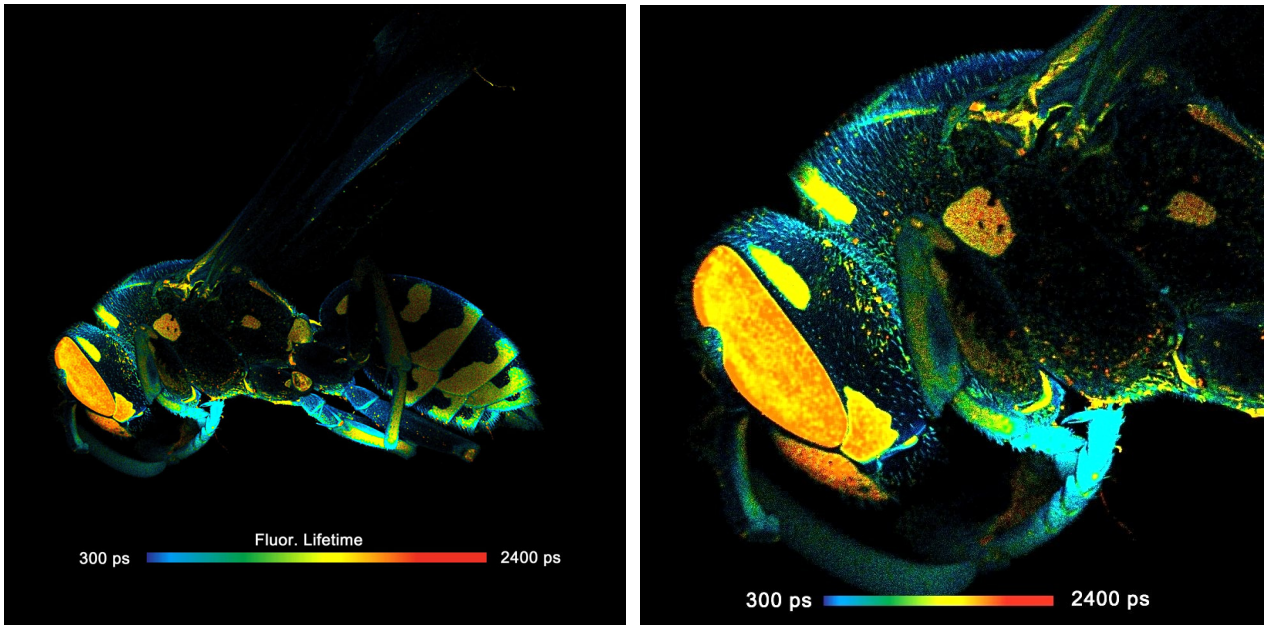


Fig. 1: FLIM of a wasp recorded in the primary image plane of a bh DCS-120 scanner. 2048x2048 pixels, 256 time channels. Left: Full-size scan, field diameter 18 mm. Right: A digital zoom into the image shown left gives an impression of the spatial resolution on the data.

## Principle

The optical principle of the DCS-MACRO system is shown in Fig. 2. The angle of the laser beam is scanned by two fast-moving galvanometer mirrors. The scan lens focuses the laser beam into an image plane shortly in front of the scanner, and simultaneously transfers the angular motion of the beam into a lateral motion in this plane [4].

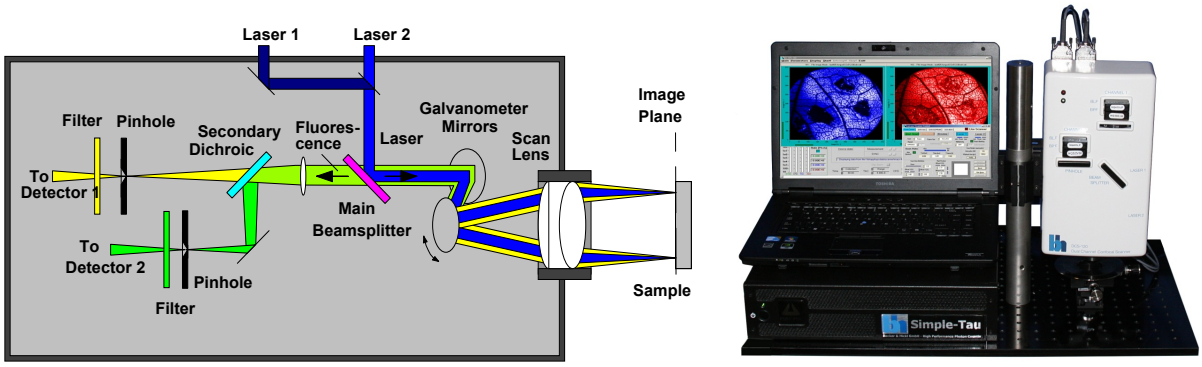


Fig. 2: Left: Principle of the DCS-120 scanner for imaging macroscopic objects. Right: Photo of the system.

The focused laser beam excites fluorescence at the surface of the sample or slightly below. The fluorescence light is collected and collimated by the scan lens, de-scanned by the galvanometer mirrors, and separated from the excitation light by the main dichroic beamsplitter. The fluorescence beam is further split into two spectral or polarisation components, and focused into pinholes. Only light that comes from the focal plane of the excitation beam can pass the pinholes efficiently. The pinholes thus suppress light that is scattered in the sample or excited outside the focal plane. Photons passing the pinholes is sent to the detectors [5, 6] through bandpass filters. FLIM data are built up from the times and locations of the photons by multi-dimensional TCSPC [2, 3].

In fact, Fig. 2 describes the known operation principle of a confocal scanner [3, 4]. It is the same as for a scanner attached to a microscope, with the difference that the microscope and thus the magnification by its objective lens is left off. The relative resolution of the images, i.e. the ratio of field diameter to the size of the point-spread function is the same as in combination with a microscope. A full-size images can, in principle, reasonably be scanned with 2048 x 2048 pixels. That means, images recorded in the scanner image plane can be amazingly rich in detail, as can be seen in Fig. 1. Acquisition times range from a few seconds for imaging with low pixel number and moderate lifetime accuracy to a few minutes for mega-pixel images and ultra-high accuracy of the decay data.

## Metabolic FLIM

Metabolic imaging by TCSPC FLIM has an enormous potential for cancer detection [18, 30], investigation of cancer origins and cancer progression [17, 19, 23,], and evaluation of the response of cells and tissues to anti-cancer drugs [16, 22, 24, 29].

Metabolic imaging is performed best by FLIM of NAD(P)H (nicotinamide adenine (pyridine) dinucleotide). It is known that the fluorescence decay function of NAD(P)H depends on the binding to proteins [12, 13, 20]. Unbound NAD(P)H has a fluorescence lifetime of about 0.3 to 0.5 ns, bound NAD(P)H has a lifetime of 1.2 ns to 3.5 ns [13]. The ratio of the amounts of bound and unbound NAD(P)H depends on the type of the metabolism. A cell can run both a reductive metabolism (glycolysis) and an oxidative one (oxidative phosphorylation). A shift from glycolysis to oxidative phosphorylation or back results in a change in the unbound/bound ratio. Thus, the

bound/unbound ratios reflect the 'Warburg Effect': In normal cells oxidative phosphorylation dominates, in cancer cells reductive glycolysis [31, 32].

Spectral separation of the signals from bound and unbound NAD(P)H is difficult, if not impossible. In FLIM data, however, the signals can be separated by double-exponential decay analysis [3, 7]. The amplitude of the fast component, a1 ('metabolic indicator'), or the ratio of the amplitudes of the decay components, a1/a2, ('metabolic ratio'), directly represent the concentration ratio of unbound/bound NAD(P)H and thus characterises the metabolic state of the tissue [3, 9, 10, 21, 27]. Having a large field of view can be extremely useful in these applications. The cell metabolism in a large piece of tissue stays intact for a longer period of time than in a thin tissue slice, post-surgery material can better be inspected for completeness of tumor excision, tumors can be investigated in their natural environment, and the effect of a tumor on the surrounding tissue can be studied.

*UV Operation of the Scanner*

A problem of NAD(P)H FLIM is the short excitation wavelength. For efficient excitation a wavelength in the range from 340 nm to 375 nm is required. Optics made of the traditional crown and flint glasses or of the modern replacements of them have poor transmission in this wavelength range. This is not a severe problem when the scanner is used in combination with a microscope. The laser power is then limited by the photostability of the sample. The applicable power is far below the maximum power of a picosecond diode laser, so that some loss in the excitation path can easily be tolerated.

For a macro scanner the situation is different. The numerical aperture of the detection beam path is much smaller than in a microscope. That means the collection efficiency is lower. Low detection efficiency must be compensated by high excitation power. Different than in a microscope, high power it not a problem for the sample because it is distributed over a large scan area. Unfortunately, the power of a picosecond diode laser is limited to a few mW. It is therefore important to minimise the losses of the laser on its way from the scanner input to the sample. We therefore designed a scan lens from novel UV-transparent glass types which recently became available. A comparison of the image intensity obtained with new UV scan lens compared to the normal VIS lens is given in Fig. 3. A FLIM image recorded with the UV lens is shown left, an image recorded with the VIS lens is shown right. The recorded intensity is 40% higher with the UV lens.

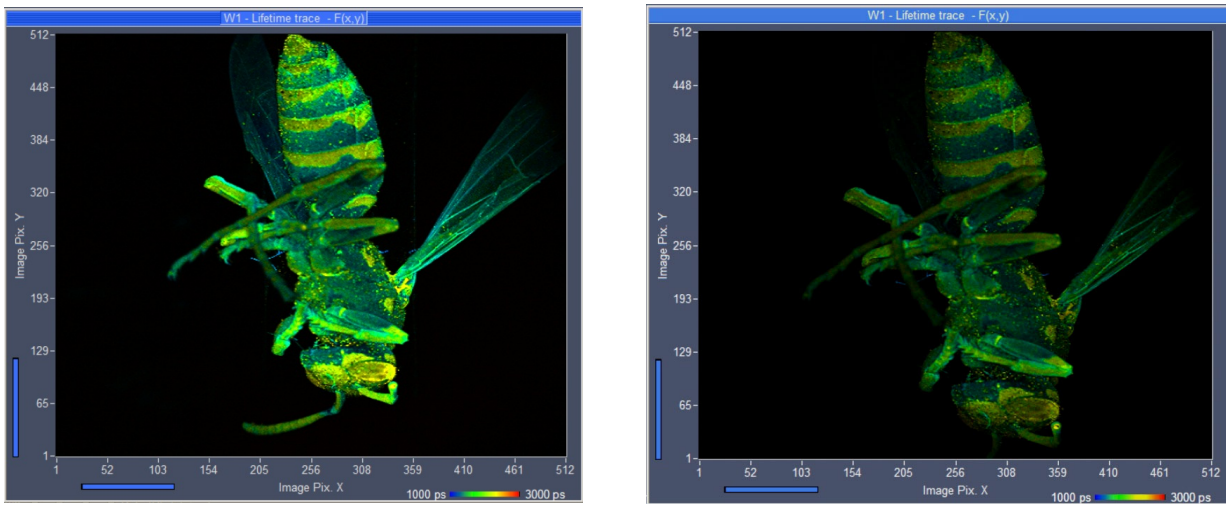


Fig. 3: FLIM of a wasp, excitation 375 nm. Recorded with the UV lens (left) and image recorded with the VIS lens (right)

## Results

### *Tumor in a Mouse*

Fig. 4 shows a FLIM image of a tumor in a mouse. The skin was removed over the tumor to provide direct optical access to the tumor tissue. The data were analysed with SPCImage NG [3, 7]. A double-exponential model was used, the image parameter is the amplitude, a1, of the fast decay component.

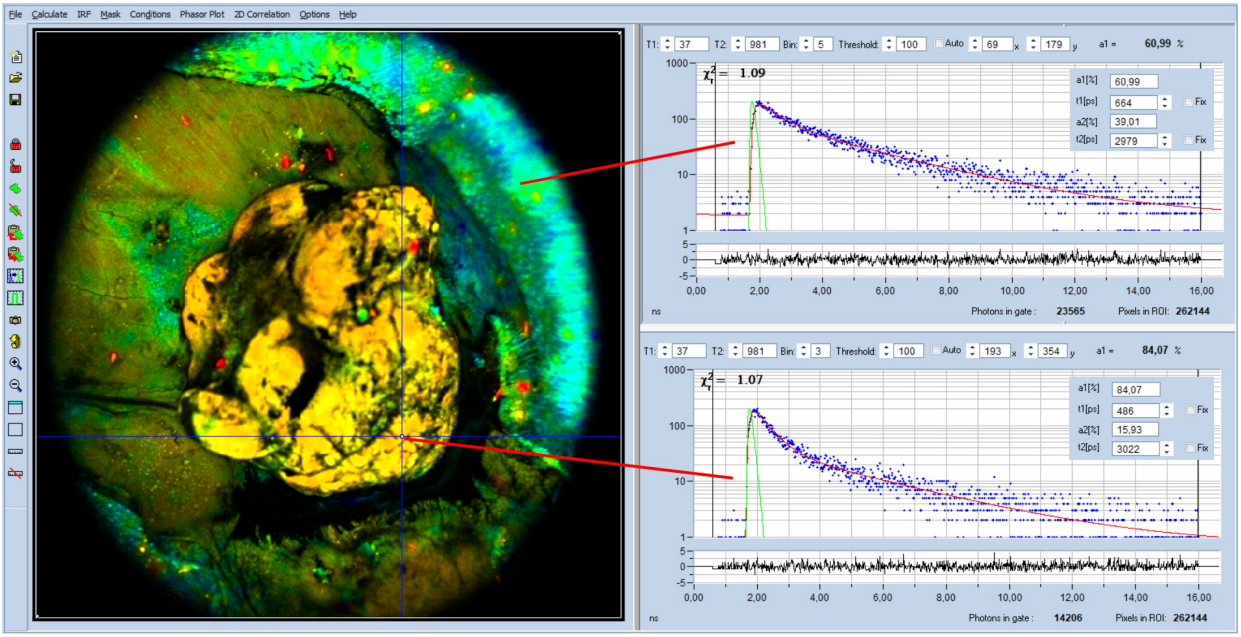


Fig. 4: Macro-FLIM data of an open tumor in a mouse. Analysis with SPCImage, double-exponential analysis, image parameter is the amplitude, a1, of the fast decay component. Decay curves in the non-tumor and in the tumor region shown on the right.

Decay curves in the non-tumor and in the tumor region are shown on the right. Visibly, the decay curve in the tumor region (lower curve) appears steeper than the curve in the non-tumor region (upper curve). The decay parameters (see insert in the curve) show the effect quantitatively: The amplitude, a1, in the tumor region is higher than in the non-tumor region. The a1 values are 84% and 61%, respectively. This is exactly what has to be expected: The amount of free NAD(P)H is higher in the tumor [3]. The result is perfectly compatible with [10] and [27], where the transition from non-tumor to tumor was found at an a1 of about 70%.

### *Glioblastoma*

Almost all types of tumor cells and tumor tissues investigated so far show identical behaviour: A tumor has an increase in a1, showing that there is more unbound NAD(P)H than in healthy tissue [3]. No so glioblastoma. Either there is no increase in a1 compared to the surrounding brain tissue, or, in contrast to other tumors, even a *decrease* in a1. The reasons of this behaviour are unknown. Of course, one may just accept that glioblastoma are in some way special. However, it is hard to believe that glioblastoma should have no metabolic shift toward glycolysis, or that this shift should not be reflected by an increase of unbound NAD(P)H. We therefore performed macroscopic FLIM measurement on excised rat brains that contained glioblastoma, see [18] for details. An example is shown in Fig. 5.

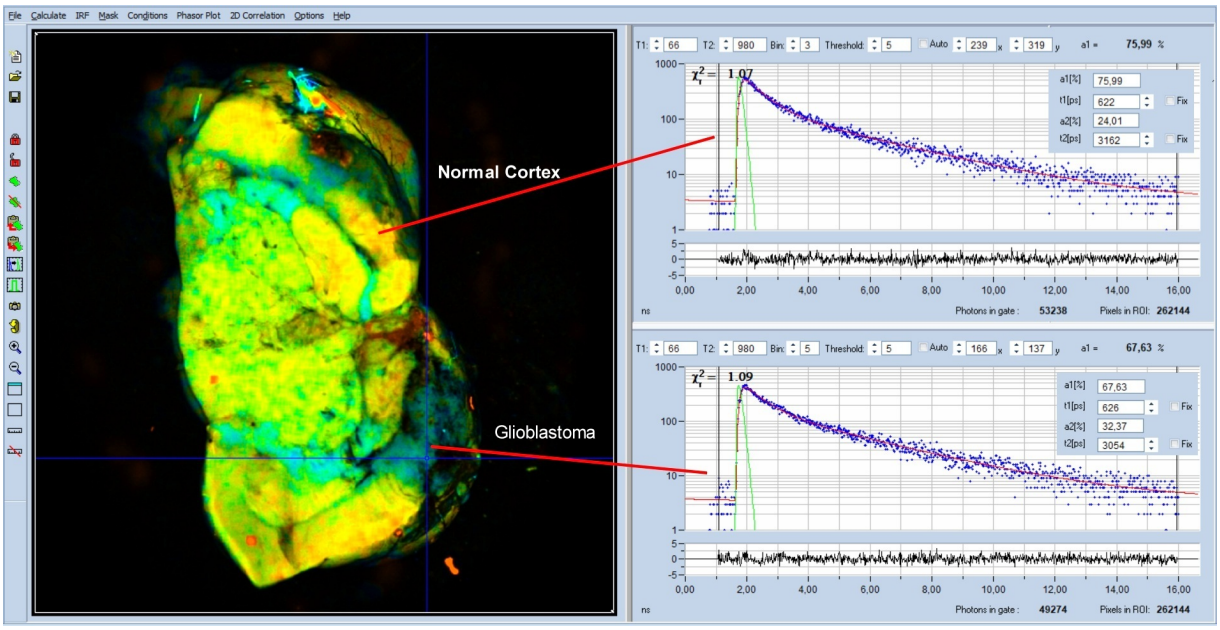


Fig. 5: MACRO-FLIM image of a rat brain with a glioblastoma. The glioblastoma is the blue area in the lower right of the image. Decay curves from a healthy region and from the tumor region are shown upper and lower right.

The glioblastoma is the blue area in the lower right of the image. Decay curves from a healthy region and from the tumor region are shown upper and lower right. Decay parameters are shown as inserts in the decay curves. Indeed, the tumor has a lower a1 than the healthy tissue: In the tumor a1 is 67%, compared to 76% in the surrounding brain tissue.

We can exclude simple instrumental artefacts or mistakes in the measurement procedure as a source of the effect. The data quality is excellent, as the decay curves in Fig. 5 show. A common mistake is detection of FAD instead of NAD(P)H. FAD can be excited at the same wavelength as NAD(P)H, and exhibits an opposite metabolic effect in a1 as NAD(P)H. However, we used an emission filter which blocked wavelengths above 475 nm. Accidental detection of FAD can therefore be excluded.

A hint towards a possible explanation is the large a1 which is observed in the healthy regions. With a1 = 76% it is in fact far in the region which is typical for tumors. Is the high a1 a general feature of brain tissue? Is it possible that in fact a1 in the normal regions is too high, and not the a1 in the tumor too low? This could potentially reverse the a1 effect.

A possible reason of high a1 could be the high metabolic activity of the brain cortex. The high energetic and biosynthetic demands of neurons and astrocytes in the brain tissue shift its metabolism toward glycolysis, accompanied by an increase in a1. Unlike the cortex, the white matter, which is composed of myelinated nerve fibres, typically has lower a1 than glioma, please see [33]. It can also not be excluded that the excised brain tissue runs into hypoxia. It would then shift its metabolism toward glycolysis, accompanied by an increase in a1. The only way to avoid this is to drastically reduce the time from excising the brain to the FLIM recording, or to record FLIM directly in the rat, either through a cranial window [1] or through an optical fibre [15].

## Possible Extensions

The system can be extended to detect FAD simultaneously with NAD(P)H. Two lasers, one for excitation of NAD(P)H and the other for FAD are multiplexed synchronously with the lines or frames of the scan, and the emission signals detected by two detectors and two parallel TCSPC

FLIM channels [9]. The corresponding control functions are implemented in the scan controller and in the SPCM data acquisition software [3, 4].

Laser multiplexing can also be used to record NAD(P)H FLIM simultaneously with FLIM of an exogenous fluorophore. This fluorophore may be used to detect changes in pH [26], concentration of special ions, protein conformation, local viscosity, or another molecular parameter [28].

Another extension is simultaneous recording of FLIM and PLIM (phosphorescence lifetime images) [8]. FLIM is then used to determine the metabolic state, PLIM to determine the oxygen partial pressure in the tissue [11, 25]. Also these functions are implemented in the DCS-MACRO standard systems. Please see [3, 4].

## Summary

The bh DCS-120 MACRO system detects FLIM from objects as large as 20 mm in diameter. The sensitivity of the system at excitation wavelengths in the near-UV region has been significantly increased by a new scan lens consisting of novel UV transmitting glass types. A 375-nm picosecond diode laser is used to excite fluorescence of NAD(P)H. The fluorescence is detected by high-speed high sensitivity hybrid detectors and recorded by multi-dimensional TCSPC. The spatial resolution of the images is about 15 µm, pixel numbers can be as large as 2048 x 2048. We have shown the performance of the system for recording metabolic FLIM of a tumor in a mouse and of glioblastoma in a rat brain. The data are analysed with SPCImage NG. Double exponential decay analysis delivers the amplitude of the fast decay component, a1, which is a direct indicator of the metabolic state of the tissue.

## References

1. B. J. Bacskai, J. Skoch, G.A. Hickey, O. Berezovska, B.T. Hyman, Multiphoton imaging in mouse models of Alzheimer's disease, Proc. SPIE, **5323**, 71-76 (2004)
2. W. Becker, Advanced time-correlated single-photon counting techniques. Springer, Berlin, Heidelberg, New York, 2005
3. W. Becker, The bh TCSPC handbook. 9th edition, Becker & Hickl GmbH (2021), available on www.becker-hickl.com. Please contact bh for printed copies.
4. Becker & Hickl GmbH, DCS-120 Confocal Scanning FLIM Systems. User handbook. www.becker-hickl.com
5. Becker & Hickl GmbH, The HPM-100-40 Hybrid Detector. Application note, available on www.becker-hickl.com
6. Becker & Hickl GmbH, Sub-20ps IRF Width from Hybrid Detectors and MCP-PMTs. Application note, available on www.becker-hickl.com
7. Becker & Hickl GmbH, SPCImage next generation FLIM data analysis software. Overview brochure, available on www.becker-hickl.com
8. Becker & Hickl GmbH, Simultaneous Phosphorescence and Fluorescence Lifetime Imaging by Multi-Dimensional TCSPC and Multi-Pulse Excitation. Application note, available on www.becker-hickl.com
9. W. Becker, A. Bergmann, L. Braun, Metabolic Imaging with the DCS-120 Confocal FLIM System: Simultaneous FLIM of NAD(P)H and FAD, Application note, available on www.becker-hickl.com (2018)
10. W. Becker, R. Suarez-Ibarrola, A. Miernik, L. Braun, Metabolic Imaging by Simultaneous FLIM of NAD(P)H and FAD. Current Directions in Biomedical Engineering 5(1), 1-3 (2019)
11. S. Kalinina, V. Shcheslavskiy, W. Becker, J. Breymayer, P. Schäfer, A. Rück, Correlative NAD(P)H-FLIM and oxygen sensing-PLIM for metabolic mapping. J. Biophotonics 9(8):800-811 (2016)
12. J.R. Lakowicz, H. Szmacinski, K. Nowaczyk, M.L. Johnson, Fluorescence lifetime imaging of free and protein-bound NADH, PNAS 89, 1271-1275 (1992)
13. J.R. Lakowicz, Principles of Fluorescence Spectroscopy, 3rd edn., Springer (2006)

14. M.N. Pastore, H. Studier, C.S. Bonder, M.S. Roberts, Non-invasive metabolic imaging of melanoma progression. Exp. Dermatol. 26, 607–614 (2017)
15. M. Lukina, A. Orlova, M. Shirmanova, D. Shirokov, A. Pavlikov, A. Neubauer, H. Studier, W. Becker, E. Zagaynova, T. Yoshihara, S. Tobita, V. Shcheslavskiy, Interrogation of metabolic and oxygen states of tumors with fiber-based luminescence lifetime spectroscopy. Optics Letters 42(4) 731-734 (2017)
16. M. M. Lukina, V. V. Dudenkova, N. I. Ignatovaa, I. N. Druzhkova, L. E. Shimolina, E. V. Zagaynovaa, M. V. Shirmanova, Metabolic cofactors NAD(P)H and FAD as potential indicators of cancer cell response to chemotherapy with paclitaxel. BBA – General Subjects 1862, 1693-1700 (2018)
17. M. M. Lukina, L. E. Shimolina, N. M. Kiselev, V. E. Zagainov, D. V. Komarov, E. V. Zagaynova, M. V. Shirmanova, Interrogation of tumor metabolism in tissue samples ex vivo using fluorescence lifetime imaging of NAD(P)H. Methods Appl. Fluoresc. 8, 014002, 1-11 (2020)
18. M. Lukina, K. Yashin, E. E. Kiseleva, A. Alekseeva, Varvara Dudenkova, E. V. Zagaynova, E. Bederina, I. Medyanic, W. Becker, D. Mishra, M. Berezin, V. I. Shcheslavskiy, M. Shirmanova, Label-Free Macroscopic Fluorescence Lifetime Imaging of Brain Tumors. Frontiers in Oncology 11, 666059, 1-11 (2021)
19. M.N. Pastore, H. Studier, C.S. Bonder, M.S. Roberts, Non-invasive metabolic imaging of melanoma progression. Exp. Dermatol. 26, 607–614 (2017)
20. R.J. Paul, H. Schneckenburger, Oxygen concentration and the oxidation-reduction state of yeast: Determination of free/bound NADH and flavins by time-resolved spectroscopy, Naturwissenschaften 83, 32-35 (1996)
21. P. M. Schaefer, S. Kalinina, A. Rueck, C.A.F. von Arnim, B. von Einem, NADH Autofluorescence - A Marker on its Way to Boost Bioenergetic Research. Cytometry Part A, 1-13 (2018)
22. A.T. Shah, K.E. Diggins, A.J. Walsh, J.M. Irish, M.C. Skala, In vivo autofluorescence imaging of tumor heterogeneity in response to treatment. Neoplasia 17, 862-870 (2015)
23. M. C. Skala, K. M. Riching, D. K. Bird, A. Dendron-Fitzpatrick, J. Eickhoff, K. W. Eliceiri, P. J. Keely, N. Ramanujam, In vivo multiphoton fluorescence lifetime imaging of protein-bound and free nicotinamide adenine dinucleotide in normal and precancerous epithelia. J. Biomed. Opt. 12 02401-1 to 10 (2007)
24. A. A. Gillette, C. P. Babiarz, A. R. Van Dommelen, C. A. Pasch, L. Clipson, K. A. Matkowskyj, D. A. Deming, M. C. Skala, Autofluorescence Imaging of Treatment Response in Neuroendocrine Tumor Organoids. Cancers (Basel). 13(8), 1873, 1-17 (2021)
25. Y. P. Parshina, A. D. Komarova, L. N. Bochkarev, T. A. Kovylina, A. A. Plekhanov, L. G. Klapshina, A. N. Konev, A. M. Mozherov, I. D. Shchechkin, M. A. Sirotkina, V. I. Shcheslavskiy, M. V. Shirmanova, Simultaneous Probing of Metabolism and Oxygenation of Tumors In Vivo Using FLIM of NAD(P)H and PLIM of a New Polymeric Ir(III) Oxygen Sensor. Int. J. Mol. Sci. 23 (2022) 10263
26. P.M. Schaefer, D. Hilpert, M. Niederschweiberer, L. Neuhauser, S. Kalinina, E. Calzia, A. Rueck, B. von Einem, C.A.F. von Arnim, Mitochondrial matrix pH as a decisive factor in neurometabolic imaging. Neurophotonics 4(4):045004 (2017)
27. R. Suarez-Ibarrola, L. Braun, P. Fabian Pohlmann, W. Becker, A. Bergmann, C. Gratzke, A. Miernik, K. Wilhelm, Metabolic Imaging of Urothelial Carcinoma by Simultaneous Autofluorescence Lifetime Imaging (FLIM) of NAD(P)H and FAD. Clinical Genitourinary Cancer (2020)
28. K. Suhling, L. M. Hirvonen, J. A. Levitt, P.-H. Chung, C. Tregido, A. le Marois, D. Rusakov, K. Zheng, Fluorescence Lifetime Imaging (FLIM): Basic Concepts and Recent Applications. In: W. Becker (ed.) Advanced time-correlated single photon counting applications. Springer, Berlin, Heidelberg, New York (2015)
29. A. J. Walsh, R. S. Cook, M. E. Sanders, L. Aurisicchio, G. Ciliberto, C. L. Arteaga, M. C. Skala, Quantitative Optical Imaging of Primary Tumor Organoid Metabolism Predicts Drug Response in Breast Cancer. Cancer Res 74, OF1-OF11 (2014)
30. A. J. Walsh, A. T. Shah, J. T. Sharick, M. C. Skala, Fluorescence Lifetime measurements of NADH in live cells and tissue. In: W. Becker (ed.) Advanced time-correlated single photon counting applications. Springer, Berlin, Heidelberg, New York (2015)
31. O. Warburg, On the origin of cancer cells. Science 123, 309-314 (1956)
32. O. Warburg, On respiratory impairment in cancer cells. Science 124, 269-270 (1956)
33. Yuzhakova D, Kiseleva E, Shirmanova M, Shcheslavskiy V, Sachkova D, Snopova L, Bederina E, Lukina M, Dudenkova V, Yusubalieva G, Belovezhets T, Matvienko D, Baklaushev V. Highly Invasive Fluorescent/Bioluminescent Patient-Derived Orthotopic Model of Glioblastoma in Mice. Front Oncol. 2022 Jul 13;12:897839. doi: 10.3389/fonc.2022.897839.